Available online at www.sciencedirect.com
ScienceDirect
Journal of Solid State Chemistry 180 (2007) 1051–1059
JOURNAL OF SOLID STATE CHEMISTRY
www.elsevier.com/locate/jssc

Crystal structure and magnetic properties of two new cobalt selenite halides: $Co_5(SeO_3)_4X_2$ (X = Cl, Br)

Richard Becker[a,*], Mladen Prester[b], Helmuth Berger[c], Ping Hui Lin[c,d], Mats Johnsson[a], Djuro Drobac[b], Ivica Zivkovic[b]

[a]*Department of Inorganic Chemistry, Stockholm University, S-106 91 Stockholm, Sweden*
[b]*Institute of Physics, P.O. Box 304, HR-10000 Zagreb, Croatia*
[c]*Institut de Physique de la Matiere Complexe, Ecole Polytechnique Fédérale de Lausanne, CH-1015 Lausanne, Switzerland*
[d]*Institute of Physics, Academia Sinica Nankang, Taipei 11529, Taiwan, ROC*

Received 25 September 2006; received in revised form 29 December 2006; accepted 30 December 2006
Available online 13 January 2007

Abstract

Two new isostructural cobalt selenite halides $Co_5(SeO_3)_4Cl_2$ and $Co_5(SeO_3)_4Br_2$ have been synthesized. They crystallize in the triclinic system space group $P-1$ with the following lattice parameters for $Co_5(SeO_3)_4Cl_2$: $a = 6.4935(8)$ Å, $b = 7.7288(8)$ Å, $c = 7.7443(10)$ Å, $\alpha = 66.051(11)^\circ$, $\beta = 73.610(11)^\circ$, $\gamma = 81.268(9)^\circ$, and $Z = 1$. The crystal structures were solved from single-crystal X-ray data, $R1 = 3.73$ and 4.03 for $Co_5(SeO_3)_4Cl_2$ and $Co_5(SeO_3)_4Br_2$, respectively. The new compounds are isostructural to $Ni_5(SeO_3)_4Br_2$.

Magnetic susceptibility measurements on oriented single-crystalline samples show anisotropic response in a broad temperature range. The anisotropic susceptibility is quantitatively interpreted within the zero-field splitting schemes for Co^{2+} and Ni^{2+} ions. Sharp low-temperature susceptibility features, at $T_N = 18$ and 20 K for $Co_5(SeO_3)_4Cl_2$ and $Co_5(SeO_3)_4Br_2$, respectively, are ascribed to antiferromagnetic ordering in a minority magnetic subsystem. In isostructural $Ni_5(SeO_3)_4Br_2$ magnetically ordered subsystem represents a majority fraction ($T_N = 46$ K). Nevertheless, anisotropic susceptibility of $Ni_5(SeO_3)_4Br_2$ is dominated at low temperatures by a minority fraction, subject to single-ion anisotropy effects and increasing population of $S_z = 0$ (singlet) ground state of octahedrally coordinated Ni^{2+}.

Keywords: Oxo-halide; Lone-pair elements; Crystal structure determination; Magnetic susceptibility; Zero-field splitting; Single-ion anisotropy

1. Introduction

Several new low-dimensional compounds have recently been found by utilizing *p*-element cations having stereochemically active lone electron pairs (e.g. Te^{4+}, Se^{4+}, and Sb^{3+}) and halide ions [1–7]. The lone-pair cations are found to most often form bonds only to oxygen in an oxo-chloride or oxo-bromide due to their small radius and high Lewis acid strength, while late transition metal cations, which are weaker Lewis acids, often form bonds to both oxygen- and halide anions in the same chemical environment.

The stereochemically active lone-pair will cause a one-sided asymmetric coordination for the lone-pair cation and it will function as a "chemical scissor" that helps to open up the crystal structure. In many cases also the halide ion acts as a terminating species and resides together with the lone-pairs in large non-bonding regions of the structure. Te^{4+} is known to take two main coordination polyhedra; the tetrahedral [TeO_3E] coordination or the [$TeO_{3+1}E$] distorted trigonal bipyramid coordination (E being the two valence lone pair electrons occupying a sp^3 hybridized orbital), while the smaller Se^{4+} only accept the tetrahedral [SeO_3E] coordination. There are examples described where isostructural Se^{4+} and Te^{4+} analogues exist and they thus both take the tetrahedral [LO_3E] coordination; e.g. $Cu_3Bi(SeO_3)_2O_2Cl$ [8] and $Cu_3Bi(TeO_3)_2O_2Cl$ [9], but there are also examples where two compounds having analogous

*Corresponding author. Fax: +46 8 15 21 87.
E-mail address: richard@inorg.su.se (R. Becker).

0022-4596/$ - see front matter © 2007 Elsevier Inc. All rights reserved.
doi:10.1016/j.jssc.2006.12.035

chemical formulae adopt different crystal structures e.g. monoclinic $Ni_5(TeO_3)_4Br_2$ [1] and triclinic $Ni_5(SeO_3)_4Br_2$ [10].

$Ni_5(TeO_3)_4Cl_2$ and $Ni_5(TeO_3)_4Br_2$ are isostructural layered structures that crystallize in the monoclinic space group $C2/c$ [1], while the recently described compounds $Ni_5(SeO_3)_4Br_2$ and $Ni_5(SeO_3)_4Cl_2$ both are triclinic and crystallize in $P\bar{1}$, however, they have different structures [10,11].

Co^{2+} and Ni^{2+} are similar in size and Lewis acid strength and there are many examples of isostructural compounds containing either of the two cations. The aim of this paper was to look for Co^{2+} analogues to $Ni_5(SeO_3)_4Cl_2$ and $Ni_5(SeO_3)_4Br_2$. The work resulted in the title compounds, $Co_5(SeO_3)_4X_2$ (X = Cl, Br), which were found to be isostructural to $Ni_5(SeO_3)_4Br_2$. There are no previously described compound in the Co^{2+}–Se^{4+}–O–X systems (X = Cl, Br). However, a search in the ICSD database reveals some complex oxo-halide compounds that contain both Co^{2+} and Se^{4+}; $Co(HSeO_3)Cl(H_2O)_2$ and $Co(HSeO_3)Cl(H_2O)_3$ [12,13], as well as $Ba_2Co(SeO_3)_2Cl_2$ [14], and $SmCo(SeO_3)_2Cl$ [15].

The magnetic properties of compounds like $Ni_5(TeO_3)_4X_2$ and $Ni_5(SeO_3)_4X_2$ are interesting because of the varieties in the coordination of the magnetic ion (Ni) characterizing the systems, which gives rise to complex superexchange networks, and thus unpredictable collective behaviour at low temperatures. Magnetic ordering phenomena have been reported for $Ni_5(TeO_3)_4X_2$ [1] and $Ni_5(SeO_3)_4Br_2$ [10]. Effective magnetic dimensionality (reduced at least in $Ni_5(TeO_3)_4X_2$ due to the layered structure), influence of local environment (through zero-field splitting scheme), magnetic frustration, etc., are all expected to participate in the sort and properties of the magnetic ground state. In view of our recent study on the layered Co^{2+} system $Co_7(TeO_3)_4Br_6$ revealing strong single-ion anisotropy effects [16], it would be also very interesting to study the magnetic properties of Co^{2+} analogues to the $Ni_5(TeO_3)_4X_2$ and $Ni_5(SeO_3)_4Br_2$ systems. The latter represents an independent motivation for the work presented below.

2. Experimental

2.1. Synthesis

$Co_5(SeO_3)_4Cl_2$, $Co_5(SeO_3)_4Br_2$, and $Ni_5(SeO_3)_4Br_2$ were all synthesized via chemical vapour transport reactions. The starting materials were; CoO (Alfa Aesar 99.999%), SeO_2 (Alfa Aesar 99.4%), $CoCl_2$ (Alfa Aesar 99.9%), $CoBr_2$ (Alfa Aesar 99.99%), NiO (Alfa Aesar 99.998%) and $NiBr_2$ (Aldrich 99.99 + %).

The single crystals were grown from the off-stoichiometric molar ratios $CoO:SeO_2:CoCl_2 = 4:3:1$, $CoO:SeO_2:CoBr_2 = 8:6:3$ and $NiO:SeO_2:NiBr_2 = 4:8:2$, respectively. The transport reactions were performed in closed and evacuated silica ampoules. To reduce the water content to a reproducible amount, the ampoules ($l = 250$ mm, $d = 20$ mm) were heated (1000 °C/10 h) under vacuum (10^{-5} Torr) before filling and sealing. The off-stoichiometric powder was introduced at one side, and the tube was then again evacuated. HCl or HBr electronic grade gas was introduced at room temperature into the tube that was subsequently sealed off. As the tube was gradually moved into the furnace, a large quantity of the mixture reacted. The temperatures of the two ends of the tubes were; 550–350 °C for $Co_5(SeO_3)_4Cl_2$, 600–500 °C for $Co_5(SeO_3)_4Br_2$ and 750–700 °C for $Ni_5(SeO_3)_4Br_2$. After some weeks (five for the cobalt compounds and two for the nickel compound), two different kinds of single crystals were observed in each ampoule: (i) for $Co_5(SeO_3)_4Cl_2$; deep purple single crystals with maximum size of $8 \times 4 \times 0.2\,mm^3$ grew in the centre of the ampoule at the temperature around 450–500 °C and some single crystals of $CoCl_2$ had grown in the cold end of the ampoule, together with an uncharacterized blue-violet crystalline powder; (ii) for $Co_5(SeO_3)_4Br_2$; deep purple single crystals with a maxim size of $10 \times 4 \times 0.2\,mm^3$ grew in the centre of the ampoule at the temperature around 500–570 °C and some crystals of $CoBr_2$ had grown a the cold end of the ampoule together with an uncharacterized blue-violet crystalline powder; (iii) for $Ni_5(SeO_3)_4Br_2$; orange single crystals with a maximum size of $6 \times 3 \times 0.2\,mm^3$ grew at the cold end of the ampoule and some crystals of $NiSeO_3$ had grown in the centre of the ampoule together with an uncharacterized yellow-orange crystalline powder.

The synthesis products were characterized in a scanning electron microscope (SEM, JEOL 820) with an energy-dispersive spectrometer (EDS, LINK AN10000) confirming the presence and stoichiometry of Ni, Co, Se, Cl and Br.

2.2. Crystal structure determination

Single-crystal X-ray data were collected on an Oxford Diffraction Xcalibur3 diffractometer using graphite-monochromatized Mo $K\alpha$ radiation, $\lambda = 0.71073$ Å. The intensities of the reflections were integrated and Gaussian face-indexing absorption correction was done using the software supplied by the manufacturer [17]. The crystal structures were solved by direct methods using the program SHELXS97 [18] and refined by full matrix least squares on F^2 using the program SHELXL97 [19]. All atoms were refined with anisotropic displacement parameters. Experimental parameters for $Co_5(SeO_3)_4X_2$ (X = Cl, Br) are reported in Table 1.

2.3. Magnetic properties

Magnetic ac-susceptibility data were measured with a CryoBIND system in a small-applied ac magnetic field (1 Oe typically, at the frequency of 430 Hz). Orientation of the single-crystalline samples with respect to the applied field was achieved by positioning the rectangular crystalline

platelets on the sapphire sample holder. Directions of crystalline axes, with respect to sample axes, have been determined by X-rays. Measurements were taken in a continuous-sweep temperature-heating mode at a typical rate of 1.5 K/min.

3. Results and discussion

3.1. Crystal structure

The new compounds $Co_5(SeO_3)_4X_2$ (X = Cl, Br) crystallize in the triclinic system, space group $P-1$ and they were found to be isostructural to $Ni_5(SeO_3)_4Br_2$ [10]. Experimental parameters, atomic coordinates and selected interatomic distances are reported in Tables 1–3, respectively. The structure description below is based on $Co_5(SeO_3)_4Cl_2$. Single crystals of $Ni_5(SeO_3)_4Br_2$ was also synthesized for comparative magnetic measurements; the unit cell for these crystals was found to be a = 6.4340(7) Å, b = 7.6397(8) Å, c = 7.6666(8) Å, α = 68.010(10)°, β = 74.120(9)° and γ = 81.430(9)°, that are close to the previously reported values [10].

Table 1
Crystal data for $Co_5(SeO_3)_4X_2$ (X = Cl, Br)

Empirical formula	$Co_5(SeO_3)_4Cl_2$	$Co_5(SeO_3)_4Br_2$
Formula weight	873.39	962.31
Temperature	292(3)	292(3)
Wavelength	0.71073	0.71073
Crystal system	Triclinic	Triclinic
Space group	$P-1$	$P-1$
Unit cell dimensions	a = 6.4935(8) Å	a = 6.4897(9) Å
	b = 7.7288(8) Å	b = 7.7574(10) Å
	c = 7.7443(10) Å	c = 7.7552(10) Å
	α = 66.051(11)°	α = 66.850(13)°
	β = 73.610(11)°	β = 73.960(12)°
	γ = 81.268(9)°	γ = 81.350(11)°
Volume (Å^3)	340.46(8)	344.62(9)
Z	1	1
Density (calculated) (g cm^{-3})	4.260	4.637
Absorption coefficient (mm^{-1})	17.105	22.308
Absorption correction	Gaussian	Gaussian
F(000)	401	437
Crystal colour	Purple	Purple
Crystal habit	Needle	Needle
Crystal size (mm^3)	0.127 × 0.062 × 0.020	0.237 × 0.080 × 0.019
θ range for data coll.	4.26–29.91°	4.23–29.93°
Index ranges	$-8 \leqslant h \leqslant 9$	$-9 \leqslant h \leqslant 9$
	$-9 \leqslant k \leqslant 10$	$-10 \leqslant k \leqslant 10$
	$0 \leqslant l \leqslant 10$	$-10 \leqslant l \leqslant 6$
Reflections collected	1890	3047
Independent reflections	1644 [R(int) = 0.0802]	1708 [R(int) = 0.0972]
Completeness to θ = max° (%)	96.3	96.3
Refinement method	Full-matrix least squares on F^2	Full-matrix least squares on F^2
Data/restraints/parameters	1890/0/107	1924/0/107
Goodness-of-fit on F^2	1.030	1.042
Final R indices [$I > 2\theta(I)$]	$R1$ = 0.0373	$R1$ = 0.0407
	w$R2$ = 0.0891	w$R2$ = 0.1126
R indices (all data)	$R1$ = 0.0414	$R1$ = 0.0450
	w$R2$ = 0.0909	w$R2$ = 0.1155
Largest diff. peak and hole (e Å^{-3})	2.230 and −1.914	1.666 and −1.079

The structure can be regarded as layered where the layers are made up of corner- and edge sharing [CoO_5Cl]-octahedra. The layers are connected by [CoO_4Cl_2] and [SeO_3] groups, see Fig. 1.

There are two crystallographically different Se^{4+} positions and three crystallographically different Co^{2+} positions. Both Se^{4+} cations have the classical tetrahedral [SeO_3E] coordination, where E designates the two valence electrons occupying a non-bonding orbital, with Se–O distances ranging from 1.688(3) to 1.720(3) Å for Se(1) and Se(2). The E positions have been calculated assuming an average Se–E distance of 1.22 Å according to Galy et al. [20].

All three Co^{2+} cations have distorted octahedral coordinations. Co(1) and Co(3) both have a [CoO_5Cl] coordination with Co–O distances ranging from 2.043(3) to 2.156(3) Å and the Co–Cl distance are 2.606(1) and 2.998(2) Å, respectively. Co(2) has a [CoO_4Cl_2] coordination with the oxygen atoms in the square plane with Co–O distances in the range 2.018(3) to 2.071(3) Å and the Co–Cl distances at 2.553(1) Å.

The [Co(1)O_5Cl] and [Co(2)O_5Cl] polyhedra are connected via edge sharing to form chains running along [110]. The chains are connected via corner sharing at the Cl anions to form the layers, see Fig. 2. The layers are connected via the [Co(3)O_4Cl_2] octahedra and also via the [SeO_3E] tetrahedra to form the three dimensional structure. The lone-pairs of Se^{4+} can, together with the Cl^- anions, be observed as pointing towards non-bonding regions and such channels have developed along [001] and [−110].

Bond valence sum calculations (BVS) were made using the following R_0 values; 1.811 for Se–O bonds [21], 1.685 for Co–O bonds [22], 2.01 for Co–Cl bonds [23] and 2.196 for Co–Br bonds [24]. BVS gives adequate results for all ions, although the halide gets a bit too low value, see Tables 2a,b. The differences in between the two compounds are actually very small. The general trend is an expected increase in Co–X distances when going from Cl to Br, although this is not the case in the Co(1)–X distance that actually decreases slightly for the Br-phase.

3.2. Magnetic properties

Magnetic properties of $Co_5(SeO_3)_4X_2$ single crystals have been studied by low-field ac susceptibility. Application of small measuring fields in magnetic susceptibility measurements is advantageous in studies of spontaneous magnetic orderings, i.e. magnetic phase transitions as well as in cases when Zeeman energy in stronger applied field becomes comparable with weak interactions (like zero-field splitting

Table 2a
Atomic coordinates and equivalent isotropic displacement parameters for $Co_5(SeO_3)_4Cl_2$

Atom	Wyck.	x	y	z	U_{eq}[a] (Å^2)	BVS[b]
Co(1)	*2i*	0.12311(9)	−0.30212(8)	0.41884(9)	0.0120(2)	1.83
Co(2)	*2i*	−0.67975(9)	−0.12933(8)	0.65723(9)	0.0114(2)	1.83
Co(3)	*1a*	0	0	0	0.0103(2)	1.98
Se(1)	*2i*	−0.79197(6)	0.17405(6)	0.22073(6)	0.0096(2)	4.02
Se(2)	*2i*	−0.34470(6)	−0.30682(6)	0.31961(6)	0.0092(2)	4.02
Cl	*2i*	−0.1845(2)	0.3235(2)	−0.0294(2)	0.0226(3)	0.50
O(1)	*2i*	−0.5799(5)	−0.3006(4)	0.4846(5)	0.0116(6)	1.92
O(2)	*2i*	−0.6408(5)	0.1014(4)	0.3848(4)	0.0121(6)	2.08
O(3)	*2i*	−0.8346(5)	−0.0328(4)	0.2050(4)	0.0124(6)	1.99
O(4)	*2i*	−0.2644(5)	−0.0802(4)	0.2214(4)	0.0122(6)	2.06
O(5)	*2i*	−0.1709(5)	−0.4102(4)	0.4661(5)	0.0126(6)	2.05
O(6)	*2i*	−1.0376(5)	0.2054(5)	0.3601(5)	0.0140(6)	2.09

[a] U(eq) is defined as one-third of the trace of the orthogonalized U tensor.
[b] Bond valance sum calculations has been performed according to Brown et al. [21].

Table 2b
Atomic coordinates and equivalent isotropic displacement parameters for $Co_5(SeO_3)_4Br_2$

Atom	Wyck.	x	y	z	U_{eq}[a] (Å^2)	BVS[b]
Co(1)	*2i*	0.1258(1)	−0.3039(1)	0.4171(1)	0.0111(2)	1.83
Co(2)	*2i*	−0.6776(1)	−0.1263(1)	0.6534(1)	0.0108(2)	1.87
Co(3)	*1a*	0	0	0	0.0099(2)	2.02
Se(1)	*2i*	−0.79504(8)	0.17109(7)	0.22445(7)	0.0090(2)	4.07
Se(2)	*2i*	−0.34400(8)	−0.30647(7)	0.31635(7)	0.0087(2)	4.05
Br	*2i*	−0.2040(1)	0.33895(8)	−0.03423(8)	0.0193(2)	0.62
O(1)	*2i*	−0.5779(6)	−0.2991(5)	0.4798(5)	0.0106(7)	1.94
O(2)	*2i*	−0.6440(6)	0.0994(5)	0.3871(5)	0.0117(7)	2.11
O(3)	*2i*	−0.8397(6)	−0.0331(5)	0.2078(5)	0.0118(7)	2.00
O(4)	*2i*	−0.2633(6)	−0.0813(5)	0.2192(5)	0.0116(7)	2.02
O(5)	*2i*	−0.1702(6)	−0.4077(5)	0.4603(6)	0.0126(7)	2.06
O(6)	*2i*	−1.0400(6)	0.2024(6)	0.3639(5)	0.0123(7)	2.08

[a] U(eq) is defined as one-third of the trace of the orthogonalized U tensor.
[b] Bond valance sum calculations has been performed according to Brown et al. [21].

energy) characterizing the system. As demonstrated below, both of these reasons play a role in the investigated compounds. An applied field in the range of 0.4–2 Oe was used in the reported measurements. The results are shown in Figs. 3–6.

Susceptibility measurements were performed in magnetic fields oriented along three orthogonal directions in order to study the anisotropy. The sample orientation was determined by the platelet-like sample morphologies. In view of the triclinic unit cell no perfect alignment of rectangular samples along crystalline axes was manageable but this fact did not prevent extraction of the characteristic anisotropy in the susceptibility. In each of the three orientations one of the crystalline axes were oriented approximately collinear with the magnetic field direction, as indicated in Figs. 3–5. Matching of the crystalline and morphological axes was performed independently by X-rays. For the purpose of the present study no precise sample alignment along the crystalline axes was required nor attempted.

As shown in Figs. 3–5 susceptibility is anisotropic in a broad temperature range. The anisotropy that continues far up into the paramagnetic range tells about the complex spin Hamiltonian that describes the magnetism of the compounds. Figs. 3 and 4 show that the susceptibility inverse $1/\chi$ of our samples is perfectly linear in a broad temperature range. All directional susceptibilities converge in the high temperature limit and the slope of the line characterizing the high-temperature convergence was used in the determination of the Curie constant. From the Curie constants the effective number of Bohr magnetons (μ_{eff}) was determined. For the Br- and Cl-compound the values of $\mu_{eff} \approx 4.67$ ($g_{eff} \approx 2.41$) and $\mu_{eff} \approx 4.47$ ($g_{eff} \approx 2.31$) were determined, respectively. Considering the $3d^7$ orbital configuration of Co^{2+} these results are compatible with the high-spin $S = \frac{3}{2}$ ground state favoured by Hund's rules [25]. (Corresponding values for the free $S = \frac{3}{2}$ spins are $\mu_{eff} \approx 3.87$, $g = 2$.) For the isostructural $Ni_5(SeO_3)_4Br_2$ compound (comprising Ni^{2+} ions in the $3d^8$ orbital state) on basis of Hund's rules one expects $S = 1$ spin state. From the determined Curie constant the values of $\mu_{eff} \approx 3.62$ and $g_{eff} \approx 2.56$ were found (corresponding values for the free $S = 1$ spins are $\mu_{eff} \approx 2.83$, $g = 2$) [10]. The deviations from

Table 3
Selected bond lengths (Å) $Co_5(SeO_3)_4X_2$ (X = Cl, Br)

	$Co_5(SeO_3)_4Cl_2$	$Co_5(SeO_3)_4Br_2$
Se(1)–O(2)	1.689(3)	1.682(4)
Se(1)–O(3)	1.720(3)	1.711(4)
Se(1)–O(6)	1.700(3)	1.702(4)
Se(2)–O(1)	1.701(3)	1.698(4)
Se(2)–O(4)	1.700(1)	1.707(4)
Se(2)–O(5)	1.706(3)	1.696(4)
Co(1)–X^{iv}	2.998(5)	2.985(1)
Co(1)–$O(1)^{ii}$	2.132(3)	2.119(4)
Co(1)–$O(3)^{ii}$	2.066(3)	2.088(4)
Co(1)–O(5)	2.078(3)	2.085(4)
Co(1)–$O(5)^{i}$	2.042(3)	2.068(4)
Co(1)–$O(6)^{iii}$	2.043(3)	2.052(4)
Co(2)–X^{iii}	2.606(1)	2.708(1)
Co(2)–O(1)	2.156(3)	2.169(4)
Co(2)–O(2)	2.116(3)	2.098(4)
Co(2)–$O(2)^{iii}$	2.045(3)	2.054(4)
Co(2)–$O(4)^{iii}$	2.122(3)	2.139(4)
Co(2)–$O(6)^{v}$	2.065(3)	2.061(4)
Co(3)–X	2.553(1)	2.7084(7)
Co(3)–X^{iv}	2.553(1)	2.7084(7)
Co(3)–$O(3)^{ii}$	2.071(3)	2.065(4)
Co(3)–$O(3)^{vi}$	2.071(3)	2.065(4)
Co(3)–O(4)	2.018(3)	2.021(4)
Co(3)–$O(4)^{iv}$	2.018(3)	2.021(4)

Symmetry codes: (i) $-x, -1-y, 1-z$; (ii) $1+x, y, z$; (iii) $-1-x, -y, 1-z$; (iv) $-x, -y, -z$; (v) $-2-x, -y, 1-z$; (vi) $-1-x, -y, -z$.

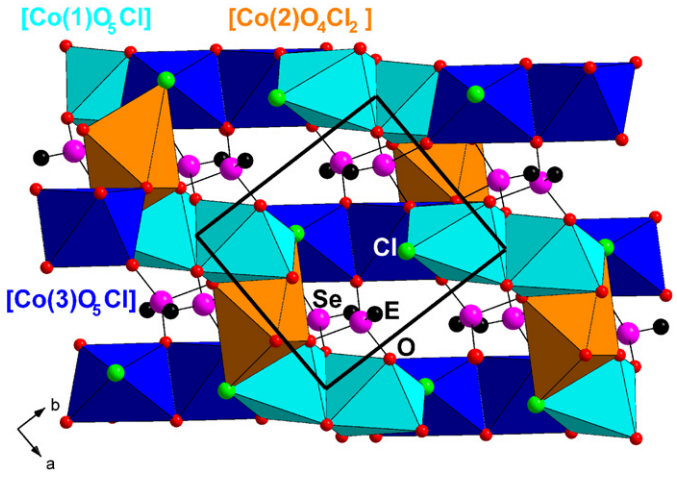

Fig. 1. $Co_5(SeO_3)_4Cl_2$ seen along the c-axis. The layers are held together by [SeO_3E] tetrahedra and [$Co(3)O_4Br_2$] octahedra.

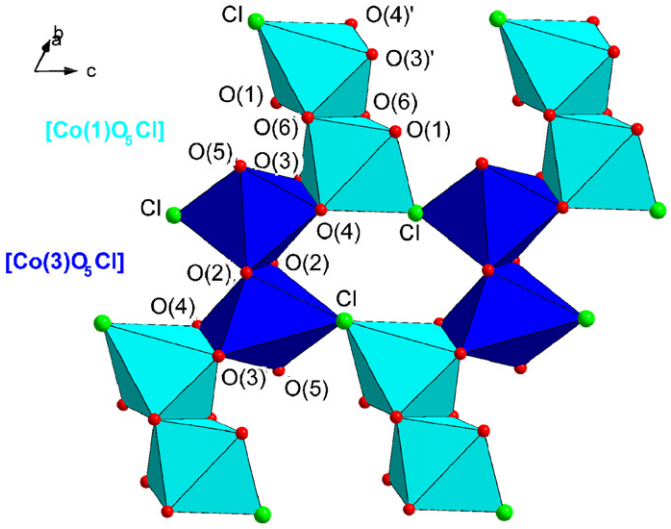

Fig. 2. The layers of $Co_5(SeO_3)_4Cl_2$ are made up of edge and corner sharing [$Co(1)O_5Cl$] and [$Co(2)O_5Cl$] octahedra. View along [−110].

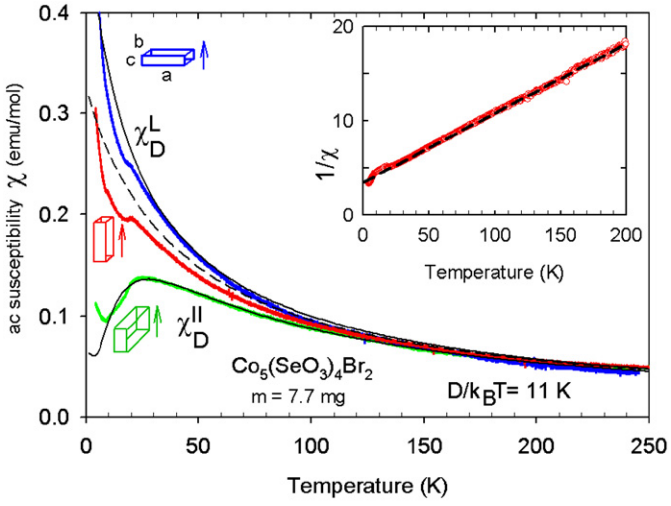

Fig. 3. AC susceptibility of a $Co_5(SeO_3)_4Br_2$ single crystal in the three orthogonal positions. The crystal shape is schematically shown and the respective directions of the crystalline axes are indicated and arrows designate the direction of the applied magnetic field, the triclinic angles have not been taken into account. A measuring field of $H_{ac} = 0.4$ Oe and frequency of 430 Hz has been applied. Curie–Weiss plot for one sample orientation is shown in the inset and in the main panel (dashed line). The solid lines in the main panel represent a one-parameter fit (in single-ion anisotropy energy D) to anisotropic susceptibility of two Kramers doublets, representing the ground ($S = \frac{1}{2}$) and the first excited states ($S = \frac{3}{2}$) for Co^{2+} ion, as calculated in [29].

the free spin values document an incomplete quenching of the orbital degrees of freedom. The evidence of orbital magnetism surviving quenching is, in turn, compatible with the susceptibility anisotropy characterizing the compounds, as discussed below. Fig. 6 presents the susceptibility data in the form of $\mu_{eff}-T$ plots. Here, the temperature-dependent μ_{eff} is determined from the standard expression, $\mu_{eff}(T) = (3k_B/N_A\mu_B^2)^{1/2}(\chi T)^{1/2}$ revealing pronounced downturn deviation from linearity in the whole temperature range.

At low temperatures the susceptibility anisotropy behaves unusually and striking. The sharp anomalies at $T_N = 18.5$ and 20 K, for $Co_5(SeO_3)_4Cl_2$ and $Co_5(SeO_3)_4Br_2$, respectively, are reminiscent of some sort of antiferromagnetic ordering. Indeed, in one particular sample direction susceptibility shows a pronounced drop, just as in a Néel-type antiferromagnet oriented along its easy axis. However, in directions orthogonal to the 'big-drop' direction the susceptibilities of $Co_5(SeO_3)_4X_2$ and

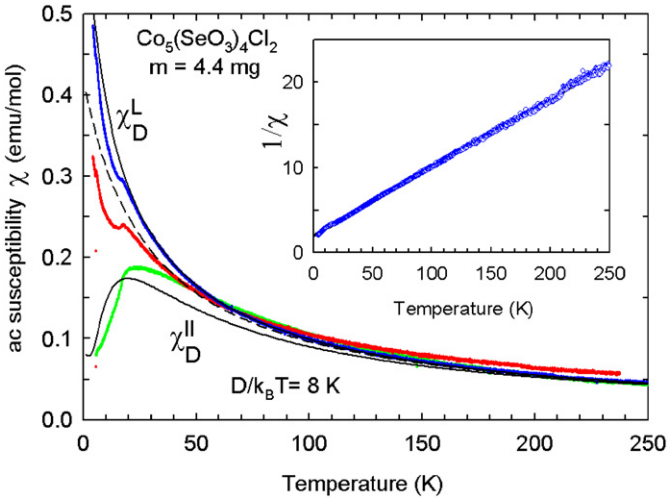

Fig. 4. AC susceptibility of a $Co_5(SeO_3)_4Cl_2$ single crystal in the three orthogonal positions. Colour of the data symbols follows the scheme illustrated in Fig. 3. Measuring field of $H_{ac} = 0.4$ Oe and frequency of 430 Hz has been applied. A C–W plot for one sample orientation is shown in the inset and in the main panel (dashed line). The solid lines in the main panel represent a one-parameter fit (in single-ion anisotropy energy D) to anisotropic susceptibility of two Kramers doublets, representing the ground ($S = \frac{1}{2}$) and the first excited state ($S = \frac{3}{2}$) for Co^{2+} ion, as calculated in [29].

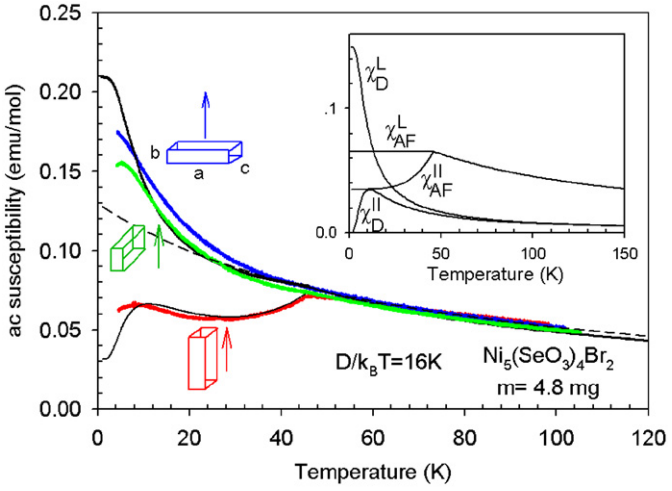

Fig. 5. AC susceptibility of a $Ni_5(SeO_3)_4Br_2$ single crystal in the three orthogonal positions. The crystal shape is schematically shown and the respective directions of the crystalline axes are indicated and arrows designate the direction of the applied magnetic field, the triclinic angles have not been taken into account. A measuring field of $H_{ac} = 2$ Oe and frequency of 430 Hz has been applied. Solid lines in the main panel represent a fit to a model of two independent magnetic subsystems. Dashed line is a Curie–Weiss fit to data. Anisotropic susceptibility (χ_D and χ_{AF}) of the two subsystems are shown in the inset. In the main panel these two susceptibilities are summed up. Susceptibility χ_D of the subsystem not involved in magnetic ordering reveals a spin singlet ($S_z = 0$) ground state.

$Ni_5(SeO_3)_4Br_2$ samples keep their high-temperature, Curie-like, rise even below T_N (Figs. 3–5). In long-range ordered antiferromagnets, the susceptibility orthogonal to the easy axis remains almost temperature independent. By lowering the temperature, it is important to note that the Curie-like

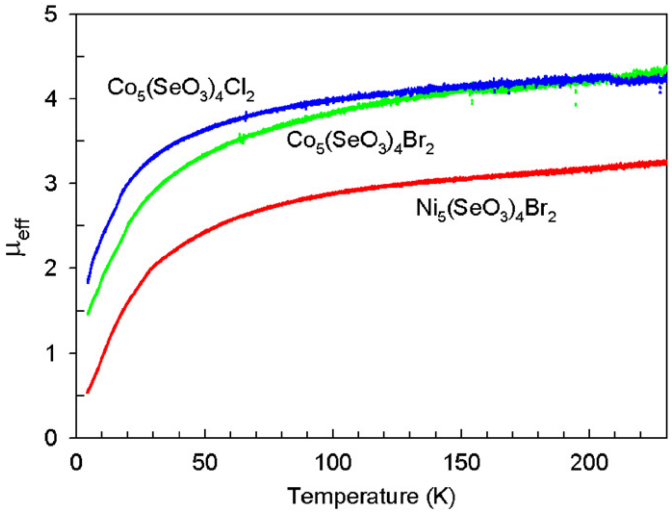

Fig. 6. Temperature dependence of μ_{eff}, effective number of μ_B. In plotting $\mu_{eff}(T)$ the same susceptibility data, otherwise used for the Curie–Weiss plots (Figs. 3–5), have been employed. Pronounced non-linearly decreasing μ_{eff} is in qualitative agreement with both the model of thermal repopulation of the effective spin states as well as with the presence of antiferromagnetic interactions.

upturn cannot be attributed to paramagnetic impurities, both because they were not detected in the X-ray studies and because the isotropic impurity contribution would have to be identified in the easy axis direction as well. In the measurements shown in Fig. 4 the upturn is entirely absent for field oriented approximately parallel to b-axis (the easy axis, green symbols in Fig. 4) while for those shown in Fig. 3 a small upturn, appearing below 7 K, can nicely be interpreted within the model of intrinsic magnetism presented below. Fig. 5 shows the corresponding results of the susceptibility-anisotropy study on an oriented $Ni_5(SeO_3)_4Br_2$ single crystal. The susceptibility of this compound has been recently reported [10], however, presenting no sample-to-field angular dependence. Qualitatively, one notes that the same susceptibility anisotropy pattern characterizing the $Co_5(SeO_3)_4X_2$ system is valid for $Ni_5(SeO_3)4Br_2$, too. From the presented susceptibility anisotropy results (Figs. 3–5) one therefore concludes that a simple antiferromagnetic (Néel) ground state is obviously not realized in $Co_5(SeO_3)_4X_2$ and $Ni_5(SeO_3)_4Br_2$.

3.3. *On the anisotropic magnetism of $Co_5(SeO_3)_4X_2$ and $Ni_5(SeO_3)_4Br_2$*

Any interpretation of the anisotropic paramagnetic susceptibility, particularly of the transition-metal ions [26], relies on non-negligible spin–orbit coupling. It introduces magnetic anisotropy either directly (through orbital magnetic contributions) or indirectly (as a mediator between the crystal–ligand–fields and the spin degrees of freedom). Usually, under combined effects of spin–orbit and crystal field interactions the degenerated ground state multiplet of a free-ion splits, without application of any magnetic field, into discrete levels allowing for different

spin states to be populated within an achievable temperature range. In cases with particularly strong spin–orbit coupling the orbital contributions introduce pronounced magnetic anisotropy relying on the anisotropic g-factor. From symmetry reasons the zero-field splitting scheme depends mainly on the ion coordination (usually octahedron or tetrahedron) and on the deformation field inevitably influencing the ion environment. The zero-field splitting is not only ion-specific but depends on number of microscopic parameters thus has to be investigated for each particular compound independently. In general, the appropriate spin Hamiltonian can be very complicated. However, in many cases a simple uniaxial single-ion anisotropy Hamiltonian (Eq. (1)) provides a reasonable insight

$$\mathscr{H}_D = D\left[S_z^2 - \frac{1}{3}S(S+1)\right] + g\mu_B \boldsymbol{H}\cdot\boldsymbol{S}. \quad (1)$$

Here, D is single-ion anisotropy energy, the z-axis is the quantization axis aligned with the high-symmetry crystalline axis, and $\boldsymbol{S}$ and $S_z{}^2$ are the usual spin operators. In the literature there are numerous examples of this spin Hamiltonian applied to the cases of both octahedral and tetrahedral coordinations [27,28]. We show here that our results can entirely be interpreted in terms of $\mathscr{H}_D$. Given the solution of the eigenvalue problem, $\mathscr{H}_D|\psi> = E_n|\psi>$, and expressing the perturbed energy level E_n in an applied magnetic field H up to second order, $E_n = E_n^{(0)} + HE_n^{(1)} + H^2E_n^{(2)} + \ldots$, one calculates magnetic susceptibility χ for N spins in unit volume (see, e.g. [26,27]) by the use of the Van Vleck equation (Eq. (2)):

$$\chi = \frac{N\sum_n[(E_n^{(1)})^2/k_BT - 2E_n^{(2)}]\exp(-E_n^{(0)}/k_BT)}{\sum_n \exp(-E_n^{(0)}/k_BT)}. \quad (2)$$

We first introduce the problem of zero-field splitting in Co^{2+} ($3d^7$) and Ni^{2+} ($3d^8$) ions, by briefly recapitulating the relevant knowledge [26,27], applying it then to interpret the presented susceptibility results (Figs. 3–6).

3.4. Co^{2+} in $Co_5(SeO_3)_4X_2$

Depending on the compound, the Co^{2+} ions can reside in six-coordinated octahedral or four-coordinated symmetry. Crystal field removes partially the degeneracy of the ^4F free-ion configuration introducing the orbital triplet Γ_4 or the orbital singlet Γ_2 ground states, for octahedral or tetrahedral Co^{2+} coordinations, respectively, [26,27]. By spin–orbit coupling these ground states are further split in such a way that the two Kramers doublets, designated as $|\pm\frac{1}{2}\rangle$ and $|\pm\frac{3}{2}\rangle$, represent the ground- and the first excited state in the cases of both symmetries. The energy scale of the separation between these two doublets, usually assigned as D, is frequently at the order of 10 K. Depending on the sign of D, Hamiltonian $\mathscr{H}_D$ favours then one of the doublets to be a ground state predominantly populated at low temperatures. In particular case of $D>0$ the effective spin state at 4.2 K is $S' = \frac{1}{2}$ while at room temperature the population of the excited level is consistent with the effective $S' = \frac{3}{2}$ spin state. Simultaneously, $\mathscr{H}_D$ favours, through spin–orbit coupling, some orbitals over the others thus introducing magnetic anisotropy. Quantitatively, the susceptibility anisotropy can be calculated by a straightforward application of the Van Vleck equation on the double-degenerate unperturbed levels $E_{1,2}^{(0)} = 0$ and $E_{3,4}^{(0)} = D$, split under the influence of Zeeman interaction into four levels ($-g\mu_B/2$, $+g\mu_B/2$, $-3g\mu_B/2$, $+3g\mu_B/2$). The results of such a calculation, for the two characteristic magnetic field directions, were published four decades ago by Van Stapele et al. [29]. The related expression, due to its length, will not be reproduced here. Our single-parameter fit (D) to the latter expression for parallel and orthogonal susceptibility is shown in Fig. 3 and 4 for $Co_5(SeO_3)_4X_2$ samples. The results are compatible with a positive D and can obviously be convincingly interpreted within the latter single-ion anisotropy model. Concerning the treatment of exchange interactions one has to point out that there is an important deviation from the original formula published in [29]. While in the original model no interaction has been assumed (thus there is a Curie-like divergence for $T = 0$ K) the basic susceptibility of $Co_5(SeO_3)_4X_2$ samples are Curie–Weiss (C–W) like (with the Weiss parameter θ being $\theta = -42$ and -30 K, for the Br- and Cl-compound, respectively). From the fact that particular directional susceptibilities all converge at high temperatures to the C–W behaviour, while the room temperature susceptibility is fairly isotropic, we conclude that (antiferromagnetic) interactions are indeed present in our system. These interactions have implicitly been taken into account in the model presented in Figs. 3 and 4 by using a $T+\theta$ temperature scale. As a consequence of the interactions there is actually AF ordering taking place in the compounds. While the global susceptibility is subject to single-ion-based constrains the sharp features in Figs. 3 and 4 are attributed to ordering of an intrinsic magnetic subsystem. From the relatively small size of these anomalies one concludes that latter magnetic subsystem involves obviously a minor fraction of spins available in the system. In view of three crystallographically different Co^{2+} positions identification of the magnetic fractions will represent an import further step in studying the magnetism of $Co_5(SeO_3)_4X_2$ compounds.

3.5. Ni^{2+} in $Ni_5(SeO_3)_4Br_2$

In $Ni_5(SeO_3)_4Br_2$ Ni^{2+} resides in octahedral coordination, which is the most interesting one from magnetic point of view [27]. In an axially deformed octahedral field a 21-fold degenerate ^3F ground state multiplet of a free-ion splits in such a way that the Γ_2 orbital singlet is the only one that can be populated at room temperatures and below. By combined action of crystal field and spin–orbit interaction Γ_2 further splits into a spin singlet $|S_z = 0\rangle$ and a doublet $|S_z = \pm 1\rangle$. As it was shown in numerous reports [27] the latter splitting can perfectly be modelled by the spin

Hamiltonian $\mathscr{H}_D$ (Eq. (1)). Either $|S_z=0\rangle$ or $|S_z=\pm1\rangle$ represents then a ground state, for $D>0$ or $D<0$, respectively. An interesting situation arises in the case of $D>0$ (singlet ground state), as realized in several Ni^{2+} compounds [27,30]. We show below that $Ni_5(SeO_3)_4Br_2$ represents a new compound revealing elements of the singlet ground state.

Again, one calculates susceptibility of the two level system starting from $E_1^{(0)}=0$ and $E_{2,3}^{(0)}=D$ as unperturbed energy levels. Applied magnetic fields lifts the remaining degeneracy in $E_{2,3}^{(0)}$ liberating altogether three levels (0, $-g\mu_B/2$, $+g\mu_B/2$). The results for susceptibility parallel and orthogonal to anisotropy axis were published by Carlin et al. [27,30] and, again, will not be reproduced here. Generic susceptibility curves, for the case $D/k_BT=16\,K$ and $S_z=\pm1$ in the high temperature limit, designated as $\chi_D^{II,L}$, are shown in the inset to Fig. 5.

In application of these result to $Ni_5(SeO_3)_4Br_2$ one has to clear out first the overlap with magnetic ordering. A pronounced and sharp susceptibility drop at $T_N=46\,K$ (Fig. 5) would be most naturally related to AF ordering. In our model, we decompose the system into two subsystems, out of which one orders antiferromagnetically at T_N while the other is subject to a zero-field splitting scheme. The susceptibility of these two independent components, designated as $\chi_D^{II,L}$ and $\chi_{AF}^{II,L}$, are shown in the inset to Fig. 5. Thus, in this model we interpret the measured susceptibility as a sum $\chi=A\chi_{AF}+(1-A)\chi_D$, where A designates the fraction of the sample participating in the long range ordering. The parameters of $\chi_{AF,D}$ were first accommodated in such a way that in the sum the experimental high-temperature C–W tail would be well-reproduced. Below AF transition in the ordering subsystem χ_{AF}^{II} was arbitrary modelled by power law (exponent $n=4$) while χ_{AF}^{L} was simply kept constant below T_N. Accommodating the main parameters of the model (A and D) to the measured susceptibility curves a surprisingly good accordance was found for the choice $A=0.9$, $D/k_BT=16\,K$. Thus, contributing just as a minor fraction (10% spins out of total) the single-ion component provides a sizable, at low temperatures even a dominant, contribution to the measured susceptibility.

3.5. Concluding remarks on the magnetism

Considering the apparent complexity in the magnetism of $Co_5(SeO_3)_4X_2$ and $Ni_5(SeO_3)_4Br_2$ the models presented above obviously reproduce the experimental results surprisingly well. In order to avoid any over-interpretation the number of free parameters were kept as low as possible. Thus, for example, no attempts to play with anisotropy (or temperature dependence) of the g-factor have been made. The parameter 'fine tuning' would certainly improve the quality of the fits further. However, the deviation of experimental results from model predictions (e.g. in Fig. 4) is primarily ascribed to incomplete alignment of the relevant sample axis along the field direction, allowing for some mixture of 'pure' parallel and orthogonal signals in the measured ones.

Evidence of a singlet ground state in $Ni_5(SeO_3)_4Br_2$, as introduced by the mechanism of zero-field splitting, attracts recently a lot of attention in the general context of quantum phase transitions [31,32]. Adding a new (inorganic) compound to the list of Ni^{2+} ground state singlets, even if such a ground state is realized in a minority phase, is certainly important. In view of the fundamental interest for inhomogeneous magnetic systems, crossing-over from classically ordered to quantum disordered ones [32], it may turn out that the decomposition of $Ni_5(SeO_3)_4Br_2$ into two intrinsic magnetic fractions could be an advantage rather than a drawback.

4. Conclusions

The crystal structures of two new isostructural selenite halide compounds $Co_5(SeO_3)_4X_2$ ($X=Cl$, Br) are described. The compounds have been synthesized via chemical vapour transport reactions in sealed evacuated silica tubes and the structures were solved from single-crystal X-ray diffraction data. Also the basic magnetic properties have been characterized and compared with the isostructural compound $Ni_5(SeO_3)_4Br_2$. The compounds crystallize in the triclinic system, space group $P\bar{1}$. Co^{2+} show distorted $[CoO_5X]$ and $[Co_4X_2]$ octahedral coordination and Se^{4+} have the classical $[SeO_3E]$ tetrahedral coordination, which includes the stereochemically active lone pair electrons (E). The structure can be regarded as layered where the layers are made up of edge- and corner sharing $[CoO_5X]$ octahedra, and further connected by $[CoO_4X_2]$ octahedra and $[SeO_3E]$ tetrahedra.

Magnetic susceptibility of $Co_5(SeO_3)_4X_2$ reveals anisotropy typical for zero-field splitting introduced by single-ion anisotropy. At high temperatures, magnetic susceptibility is compatible with the expected $S=\frac{3}{2}$ spin state of Co^{2+}, favoured by Hund's rules. However, the presented model demonstrates that the effective spins state $S'=\frac{3}{2}$ (Kramers doublet state) becomes depopulated by lowering temperature at the expense of increasingly populating effective $S'=\frac{1}{2}$ Kramers doublet. The involved single-ion anisotropy energy was found to be $D/k_BT=11\,K$ and $D/k_BT=8\,K$, for $Co_5(SeO_3)_4Br_2$ and $Co_5(SeO_3)_4Cl_2$, respectively. A similar model was applied to interpret the anisotropic susceptibility of $Ni_5(SeO_3)_4Br_2$, focusing on the possible $S_z=0$ and ±1 ground states of Ni^{2+} ion in axially deformed octahedral environment. Our results are compatible with $S_z=0$ singlet ground state in a minority magnetic subsystem, becoming populated at low temperatures. Single-ion anisotropy energy was found to be $D/k_BT=16\,K$. In both $Co_5(SeO_3)_4X_2$ and $Ni_5(SeO_3)_4Br_2$ the effective number of Bohr magnetons $\mu_{eff}(T)$ was found non-linearly decreasing by cooling, in general agreements with both the thermal repopulation of the effective spin states and the presence of antiferromagnetic interactions.

Long-range antiferromagnetic ordering is also present in the investigated compounds, permeating, however, only one subsystem of the whole magnetic system. While in $Co_5(SeO_3)_4X_2$ the latter subsystem, according to our results, represents a minor fraction in $Ni_5(SeO_3)_4Br_2$ magnetically ordered fraction dominates in its size. However, the intrinsic susceptibility behaviour of a more interesting $S_z = 0$ minority fraction is easily discernable and quantified. Identification of magnetic fractions within the available edge- and corner-sharing networks of different Co^{2+} (Ni^{2+}) octahedra is left for future investigations.

Supplementary material

Supplementary material has been sent to Fachinformationzentrum Karlsruhe, Abt. PROKA, 76344 Eggenstein-Leopoldshafen, Germany (Fax: +49 7247 808 666; E-mail: crysdata@fiz-karlsruhe.de), and can be obtained on quoting the deposit numbers CSD-416965 and 416966 for $Co_5(SeO_3)_4Cl_2$ and $Co_5(SeO_3)_4Br_2$, respectively and of the project 035-0352843-2845 from Croatian Ministry of Science, Education and Sport.

Acknowledgments

This work has in part been carried out with financial support from the Swedish Research Council. The work in Lausanne was supported by the Swiss National Science Foundation (SNSF) and by the MaNEP. The work in Zagreb was supported by the resources of the SNSF-SCOPES project.

References

[1] M. Johnsson, K.W. Törnroos, P. Lemmens, P. Millet, Chem. Mater. 15 (2003) 68–73.
[2] M. Johnsson, K.W. Törnroos, F. Mila, P. Millet, Chem. Mater. 12 (2000) 2853–2857.
[3] R. Becker, M. Johnsson, R.K. Kremer, P. Lemmens, Solid State Sci. 5 (11–12) (2003) 1411–1416.
[4] R. Becker, M. Johnsson, R. Kremer, P. Lemmens, J. Solid State Chem. 178 (2005) 2024–2029.
[5] R. Becker, H. Berger, M. Johnsson, M. Prester, Z. Marohnic, M. Miljak, M. Herak, J. Solid State Chem. 179 (2006) 836–842.
[6] R. Takagi, M. Johnsson, V. Gnezdilov, R.K. Kremer, W. Brenig, P. Lemmens, Phys. Rev. B 74 (2006) 014413.
[7] Z. Mayerová, M. Johnsson, S. Lidin, Angew. Chem. Int. Ed. 45 (2006) 5602–5606.
[8] A. Pring, B.M. Gatehouse, W.D. Birch, Am. Mineral. 75 (11–12) (1990) 1421–1425.
[9] R. Becker, M. Johnsson, Solid State Sci. 6 (6) (2004) 519–522.
[10] H.L. Jiang, J.-G. Mao, Inorg. Chem. 45 (2006) 7593–7599.
[11] Y.-L. Shen, J.-G. Mao, H.-L. Jiang, J. Solid State Chem. 178 (2005) 2942–2946.
[12] M.G. Johnston, W.T.A. Harrison, Acta Crystallogr. E 59 (2003) 62–64.
[13] M.G. Johnston, W.T.A. Harrison, Z. Anorg. Allg. Chem. 626 (2000) 2487–2490.
[14] M.G. Johnston, W.T.A. Harrison, Acta Crystallogr. E 58 (2002) 49–51.
[15] M.S. Wickleder, H. Ben Hamida, Z. Anorg. Allg. Chem. 629 (2003) 556–562.
[16] R. Becker, M. Johnsson, H. Berger, M. Prester, I. Zivkovic, D. Drobac, M. Miljak, M. Herak, Solid State Sci. 8 (2006) 836–842.
[17] CrysAlis RED 1.171.29.2 Oxford Diffraction, 2006.
[18] G.-M. Sheldrick, SHELXS-97—Program for the Solution of Crystal Structures, Göttingen, 1997.
[19] G.-M. Sheldrick, SHELXL-97—Program for the Refinement of Crystal Structures, Göttingen, 1997.
[20] J. Galy, G. Meunier, S. Andersson, E. Åström, J. Solid State Chem. 13 (1975) 142–159.
[21] I.D. Brown, D. Altermatt, Acta Crystallogr. B 41 (1985) 244–247.
[22] R.M. Wood, G.J. Palenik, Inorg. Chem. 37 (1998) 4149–4151.
[23] N.E. Brese, M. O'Keeffe, Acta Crystallogr. B 47 (1991) 192–197.
[24] C. Hormillosa, S. Healy, T. Stephen, Program Bond Valence Calculator 2.00, 1993.
[25] S. Blundell, Magnetism in Condensed Matter, Oxford University Press, New York, 2001.
[26] J.S. Griffith, The Theory of Transition Metal Ions, Cambridge University Press, London, New York, 1961.
[27] R.L. Carlin, A.J. van Duyneveldt, Magnetic Properties of Transition Metal Compounds, Springer, New York, Heidelberg, Berlin, 1977 and the references therein.
[28] R.L. Carlin, D.W. Carnegie Jr., J. Bartolomé, D. Gonzalez, L. Floria, Phys. Rev. B 32 (1985) 7476–7482.
[29] R.P. Van Stapele, H.G. Beljers, P.F. Bongers, H. Zijlstra, J. Chem. Phys. 14 (1966) 3719–3725.
[30] R.L. Carlin, K.O. Joung, A. Paduan-Filho, C.J. O'Connor, E. Sinn, J. Phys. C: Solid State Phys. 12 (1979) 293–301.
[31] V.S. Zapf, D. Zocco, B.R. Hansen, M. Jaime, N. Harrison, C.D. Batista, M. Kenzelmann, C. Niedermayer, A. Lacerda, A. Paduan-Filho, Phys. Rev. Lett. 96 (2006) 077204.
[32] T. Roscilde, S. Haas, cond-mat/0605200, and references therein.